Journal of Japan Association for Earthquake Engineering, Vol. 26, No. 2, 2026
[Technical Report (Translated Paper)]

PEAK FREQUENCY MAP OF MICROTREMOR HORIZONTAL-TO-VERTICAL SPECTRAL RATIOS: A CASE OF COMPARISON WITH THE URBAN GEOLOGICAL MAP OF THE SOUTHEASTERN AREA OF SAITAMA PREFECTURE

Ikuo CHO[1], Shigeki SENNA[2] and Susumu NONOGAKI[3]

[1] Member, Dr. Sci, Group Leader, Geological Survey of Japan, National Institute of Advanced Industrial Science and Technology, Ibaraki, Japan, ikuo-chou@aist.go.jp

[2] Member, Dr. Eng., Chief Expert Researcher, National Research Institute for Earth Science and Disaster Resilience, Ibaraki, Japan, senna@bosai.go.jp

[3] Dr. Sci, Chief Senior Researcher, Geological Survey of Japan, National Institute of Advanced Industrial Science and Technology, Ibaraki, Japan, s-nonogaki@aist.go.jp

ABSTRACT: We have identified microtremor horizontal-to-vertical spectral ratios (HVSRs) at numerous grid observation points in southeastern area of Saitama Prefecture within a rectangle with side lengths of approximately 35 km, at an average interval of about 1 km for 853 grids. Peak frequencies were read from the obtained HVSRs within a frequency range from 0.5 to 20 Hz, from which their spatial distribution was deduced (i.e., a peak frequency map). When multiple local peaks were observed within the analysis frequency range for reading, the amplitude difference between the peak and the corresponding trough was evaluated. Taking into account this information, we set a peak selection threshold and a weighting criterion and then selected a single peak to read the frequency. The resulting peak frequency map was compared with a pre-existing 3D geological structure model (i.e., the urban geological map, the UGmap) constructed based on numerous borehole data (< 7338 boreholes). They are in good agreement in their topographical and geological distributions. For example, in areas with thick alluvium (> 20 m) in the Arakawa and Nakagawa Lowlands, the peak frequency averaged a low value of 1.3 Hz, whereas in areas without alluvium, the average peak frequency was much higher at 4.7 Hz. The peak frequency of the HVSRs can be considered to be an indicator for quantifying qualitative assessments of ground conditions. The resulting peak frequency maps will be released on the website of the UGmap to enable detailed comparisons with geological distributions. We plan to construct and release similar peak frequency maps for the other regions involved in the UGmap in the future.

Keywords: *Microtremor, Geological map, Ground oscillation, Horizontal-to-vertical spectral ratios, Resonant frequency, Ground classification, Seismic hazard*

1. INTRODUCTION

Ambient vibrations (hereafter, "microtremors") refer to small-amplitude ground motions caused by various sources such as ocean waves, wind, and industrial activities. These motions propagate through the ground as elastic waves, with the propagation characteristics being dependent on the subsurface geological structure. As such, microtremors reflect site-specific ground-motion characteristics. Because microtremors are ubiquitous and can be easily recorded simply using surface-installed seismometers, microtremor measurement has long been used as a practical and cost-effective means for assessing subsurface ground conditions[1), 2)]. In particular, the peak frequency for horizontal-to-vertical spectral ratios (HVSRs)[3)] of microtremors, which can be obtained with a single three-component seismometer, is widely employed for geotechnical site categorization[4)], seismic microzonation[5)–8)], and estimating subsurface structure or providing auxiliary data for such estimations[9)–11)].

The National Institute of Advanced Industrial Science and Technology (AIST) has been using extensive borehole data to develop 3D models of the geological structure in urban areas to depths of several tens of meters, with the aim of assembling geological and geotechnical information relevant to infrastructure development, hazard/risk assessment, groundwater evaluation, and related applications[12), 13)]. The results of this effort are published as the Urban Geological Map (hereafter, "UGmap") (https://gbank.gsj.jp/urbangeol/). To date, UGmaps have been released for northern Chiba Prefecture[14)], the Tokyo metropolitan wards[15)], and southeastern Saitama Prefecture[16)]. As noted above, the objective of these UGmaps can also be partially achieved by mapping the peak frequencies of HVSRs derived from three-component microtremor measurements at the ground surface. Therefore, our aim is to construct HVSR peak-frequency maps that can be cross-referenced with existing UGmaps, to enhance the information delivered through the UGmap platform.

Based on the above considerations, we have begun evaluating the spatial distributions of HVSR peak frequencies (i.e., constructing peak-frequency maps) and comparing them with the geological distributions presented in the UGmaps. In this paper, we report these efforts related to the recently released map for southeastern Saitama Prefecture[16)]. Section 2 outlines the area targeted for modeling, its topography and geology, and the procedures used for 3D geological structure modeling. Section 3 presents a general discussion on site resonance and HVSRs, with the assumption that some UGmap users who read this report will not be earthquake engineers. Section 4 describes the microtremor data used in this study, while Section 5 explains how this data is processed (i.e., HVSR evaluation and peak-frequency map construction). Section 6 discusses the relationship between representative topographical and geological features in the area targeted for modeling and the HVSR peak frequencies.

2. URBAN GEOLOGICAL MAP FOR SOUTHEASTERN SAITAMA PREFECTURE

The Southeastern Area of Saitama Prefecture[16)] in the UGmap is enclosed within a rectangular region with sides of approximately 35 km, centered on Saitama City (Fig. 1). In this paper, we refer to this region as the model area, which is also the area for which the HVSR peak-frequency map is constructed. The northern, western, and southwestern boundaries of the area are defined by straight lines or topographic contours that run through Kuki City, Kawagoe City, and Fujimi City. The southern boundary coincides with the prefectural border with Tokyo, and the eastern boundary coincides with the prefectural borders with Chiba and Ibaraki Prefectures.

The following overview of the topography and geology of the model area is based on the explanatory text accompanying the corresponding UGmap[16)]. Interested readers are encouraged to refer to this document for more detailed descriptions and to access the UGmap website where they can browse the 3D topographic and geological structures in detail and also generate arbitrary geological cross sections

(Fig. 18 in Section 6.5).

As shown in Fig. 1, the western central part of the model area is occupied by the Omiya Upland, which extends in a north–northwest to south–southeast direction. The maximum elevation (approximately 33 m) of the upland occurs in the northwestern part around Kitamoto City, with the elevation gently decreasing toward the southeast. The upland is traversed by valley-bottom lowlands along the Shibakawa, Ayase, and Moto-Arakawa Rivers. The Omiya Upland is bounded on the west and east by the Arakawa Lowland (width 5–7 km) and the Nakagawa Lowland (width 6–14 km), respectively—both trending north–northwest to south–southeast with elevations of 5 m or less. The region exhibits evidence of large-scale artificial landform modifications, including historical river course alterations (early Edo period) and straightening of meandering channels. Further west and east of the Arakawa Lowland and Nakagawa Lowland lie the Musashino Upland and Shimosa Upland, respectively (both fall outside the model area).

The shallow subsurface geology of the model area (depths less than 100 m) comprises, from deepest to shallowest, the Middle to Upper Pleistocene Shimosa Group, Upper Pleistocene terrace deposits and the Kanto Loam Bed, and uppermost Pleistocene to Holocene alluvium. The Shimosa Group consists of terrestrial and marine beds formed through depositional cycles resulting from sea-level change that are divided, in ascending order, into the Jizodo, Yabu, Kamiizumi, Kiyokawa, Kioroshi, and Omiya Formations. In the UGmap, the younger terrace deposits are treated as a continuous depositional sequence above the Shimosa Group, and the Kanto Loam Bed is treated as covering soil. The Arakawa and Nakagawa Lowlands are underlain by thick alluvium, whose basal gravel layers are estimated to start at elevations of −50 to −20 m and −60 to −30 m, respectively.

In the UGmap, the geological features above are modeled based on reference borehole (hereafter, standard borehole) data created for establishing standard stratigraphic frameworks as well as a large amount of borehole data produced in public construction works (hereafter, public borehole data). In other words, from the standard borehole data, 1D geological classifications (stratigraphic divisions) can be obtained based on tephra, microfossils, and lithofacies analyses. It is possible to reconstruct the 3D geological structure in the vicinity of standard borehole sites by correlating these divisions with lithofacies data from public borehole datasets. Specifically, the basal elevation of each geological layer is modeled through spline interpolation. In Section 6 where we compare the thicknesses of geological units and peak frequencies, the term “geological unit thickness” refers to the elevation difference between the spline-modeled basal surfaces.

Because public borehole logs are generated in response to various societal needs, many of them do not reach the deepest stratigraphic horizons represented in the UGmaps. The number of borehole logs available for modeling basal elevations increases with decreasing depth from the surface—especially for areas underlain by alluvium. Specifically, whereas 521 borehole logs were used to model the basal surface of the deepest unit, the Yabu Formation, 4,402 logs were used to model the basal surface of the uppermost Pleistocene Omiya Formation, and 7,338 logs for the basal surface of the alluvium. In some instances, although it is not possible to determine the basal surface elevation, overlying or underlying geological units can be identified. In such situations, the basal surface is modeled by imposing inequality constraints that define upper and/or lower limits of the elevation of the basal surface. For example, a constraint such as “the basal surface of the lower part of the Kioroshi Formation must lie below the borehole termination depth” is applied.

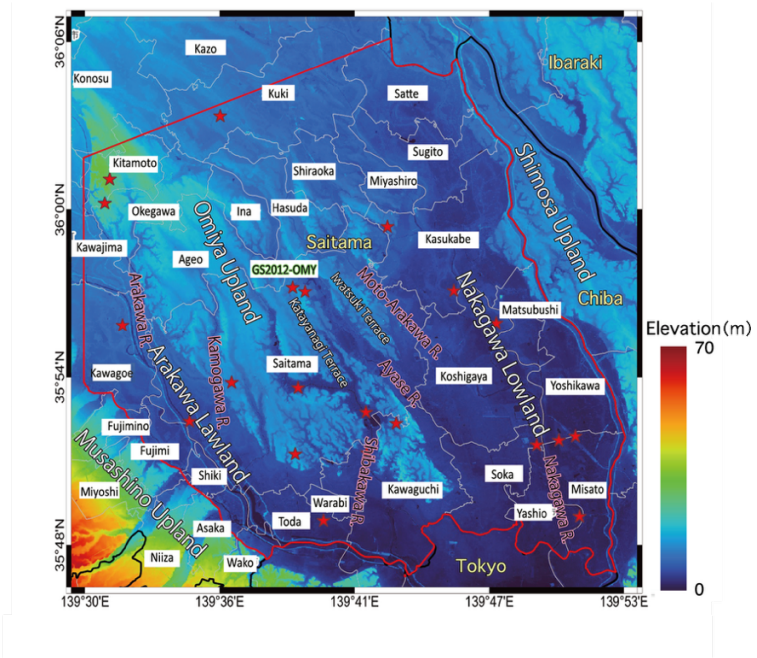

Fig. 1 Model area of Southeastern Area of Saitama Prefecture UGmap[16] (red line: model area; star symbols: standard borehole sites; elevation data and administrative boundaries are based on Fundamental Geospatial Data from the Geospatial Information Authority of Japan)

3. SITE RESONANCE AND MICROTREMOR HVSRS

When a propagating seismic wave (S-wave) enters vertically from below into a two-layered ground structure in which a soft sediment overlies a stiff layer, the seismic motion may be strongly amplified at certain frequencies. This phenomenon is referred to as site resonance, and the corresponding frequency is known as the resonant frequency[17]. In locations where the soft layer is thick or is very soft (i.e., with a lower S-wave velocity), the site resonant frequency tends toward lower frequencies. Conversely, in locations where the soft layer is thin or relatively stiff (i.e., a higher S-wave velocity), the resonant frequency tends toward higher frequencies. Practically, that means that the resonant frequency can be used to evaluate the impact of a shallow soft layer on the ground response. For example, according to the Specifications for Highway Bridges[4], sites with a resonant frequency (referred to therein as the fundamental natural period) higher than 5.0 Hz are classified as Ground Type I, sites with frequencies below 1.7 Hz as Ground Type III, and those in between as Ground Type II. For simplicity, this paper refers to these as “good ground,” “soft ground,” and “intermediate ground,” respectively. However, it should be kept in mind that these terms only pertain to the classification based on site resonant frequency. In addition, as bedrock lacks an overlying soft layer, it theoretically should not exhibit resonance. In practice, however, near-surface bedrock, which has undergone some weathering, is comparatively “soft” and exhibits observable resonance. In this study, we therefore assume that the shallow subsurface throughout the study area is comparatively “soft,” regardless of location.

The horizontal-to-vertical spectral ratio (HVSR) is defined as the ratio of the horizontal to vertical amplitudes or powers evaluated using the three-component waveforms obtained from single-point microtremor measurements (i.e., observations conducted with one seismometer placed on the ground surface). The HVSR peak frequency (f_p) is empirically known to provide a good approximation of the site resonant frequency (f_0)[18] (Fig. 2). Therefore, the spatial distribution in f_p can be interpreted as a first-order approximation of the spatial distribution in the influence of the soft layer—namely, its degree

of softness or its thickness[6]. HVSRs exhibit a pronounced peak when the impedance (product of density and S-wave velocity) contrast between the soft layer and the underlying basement is large; smaller contrasts result in lower peaks. In bedrock areas, the peak is often very weak or indistinct.

The frequency band for ground motions that directly cause earthquake damage is generally in the range of 0.1–10 Hz. Within this band, resonance phenomena occur at frequencies higher than and lower than 0.5–1 Hz related to the shallow subsurface (sediments above the engineering bedrock, typically to depths of several tens of meters) and the deep subsurface (sediments above seismic bedrock, at depths ranging from roughly 10 to 3000 m) , respectively. Here, seismic bedrock refers to the top of the crustal layer with an S-wave velocity of approximately 3 km/s, while engineering bedrock is defined as the horizon with an S-wave velocity of 300–700 m/s[19]. Correspondingly, HVSRs exhibit two types of peaks on either side of 0.5–1 Hz: lower-frequency peaks generated by the deep subsurface structure and higher-frequency peaks generated by the shallow subsurface structure (Fig. 3). In areas with thick soft layers, the resonant frequency caused by the shallow subsurface tends to be lower, often resulting in a prominent peak near 1 Hz[8]. Considering that wooden houses are known to be highly vulnerable to ground motions around 1 Hz[20], heightened attention should be paid to the potential for increased earthquake damage in such areas.

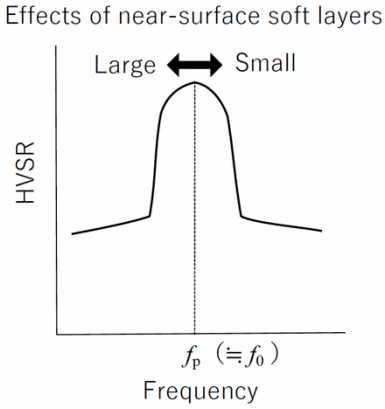

Fig. 2 Relationship between HVSR peak frequency and degree of influence of near-surface soft layers

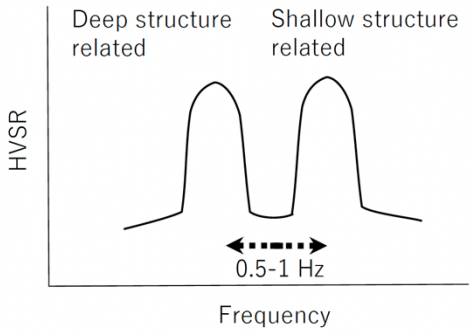

Fig. 3 Two peaks observed in HVSR

4. MICROTREMOR DATA

Microtremors within the model area of the Southeastern Area of Saitama Prefecture UGmap[16] were measured by the National Research Institute for Earth Science and Disaster Resilience at 838 grid points, arranged with an approximate spacing of 1 km[11]. Together with 15 additional measurements obtained independently by the AIST, we used a total of 853 microtremor records to evaluate the spatial distribution of HVSR peak frequency (f_p) (Fig. 4).

Microtremors were measured at each site using a measurement array whereby microtremors were measured simultaneously by using multiple seismometers. Two sizes of array were employed: miniature (radius of 0.6 m) and small (approximate radius of 10 m) arrays. These two array types were deployed concurrently using six three-component servo accelerometers (JU410, Hakusan Corporation). Microtremor waveforms were recorded using these arrays during the daytime at sampling frequencies of either 100 or 200 Hz over a period of approximately 15 minutes. This observation protocol was

employed uniformly across all 853 measurement sites.

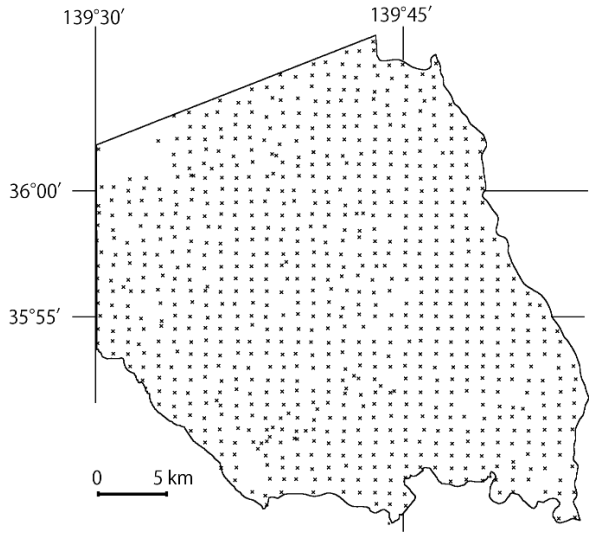

Fig. 4 Distribution of microtremor measurement sites in model area (see Fig. 1)

5. METHODS

5.1 Spectral analysis

For records obtained from each seismometer, the power spectral density was estimated for each component using a direct method based on a fast Fourier transform (FFT), where ensemble averaging combined with spectral smoothing in the frequency domain was employed[21]. Multiple segments of 10.24 or 20.48 s were extracted from the waveforms, while segments with transient noise (such as sudden pulses caused by passing vehicles) were excluded from the extraction. These extracted segments were then subjected to a FFT and used for ensemble averaging. For spectral smoothing in the frequency domain, frequency-dependent windows whose bandwidth increased with frequency were used to stabilize spectral estimates[21].

HVSR was defined as the horizontal-to-vertical power spectral ratio, computed by dividing the sum of the power spectra of the two horizontal components by that of the vertical component. Six spectra of HVSR corresponding to the six seismometers comprising the measurement array were obtained for each site. These spectra were averaged arithmetically at each frequency to derive a representative spectrum of HVSR for the site. As such, this representative spectrum can be regarded as a spatial average over a radius of about 10 m, weighted toward the location of the miniature array.

5.2 Peak frequency (f_p) determination

To identify HVSR peaks and thereby determine f_p, we restricted our evaluation to the frequency range $[f_{ll}, f_{ul}]$. Specifically, the limits were set to f_{ll} = 0.5 Hz and f_{ul} = 20 Hz. According to the specifications of the seismometers used for the microtremor measurements, this frequency band provides a flat response to ground movement and is sufficiently reliable. The upper frequency limit was chosen to constrain our evaluation to the band most commonly examined in earthquake engineering studies of HVSRs. The

lower frequency limit was imposed with the goal of capturing the relationship between f_p and the shallow-subsurface model (i.e., UGmap).

In practice, HVSRs are not as simple as that shown in Fig. 2 and often exhibit local peaks such as those indicated by the blue and red arrows in Fig. 5. Even in such cases, it is reasonable to treat the frequency corresponding to the maximum spectral amplitude within the target frequency range $[f_{ll}, f_{ul}]$ as f_p (Fig. 5a). However, HVSRs tend to show higher amplitudes at lower frequencies (Fig. 5b).

While the causes of this trend are not clear, possible explanations include leakage of deep-subsurface effects and the predominance of $1/f$ noise. "Leakage" of deep-subsurface effects refers to situations where the peak frequencies associated with the deep and shallow subsurface layers (Fig. 3) are close to each other, are broad, and have gently sloping flanks. In such cases, the peaks may overlap and influence each other. The flank on the high-frequency side of the lower-frequency peak tends to gradually decrease in amplitude with increasing frequency. If this trend extends to the higher-frequency peak, this peak may appear elevated because it rides on top of this trend[22]. $1/f$ noise refers to noise whose intensity is proportional to $1/f$ (or more generally $1/f^{\alpha}$, where α is a constant between 0 and 2[23]). Such noise is commonly observed in a wide range of physical phenomena and is caused by various sources, including electrical noise generated by recording instruments such as seismometers[24]. If $1/f$ noise with random α values is present in each of the three components of the seismometer, the HVSRs are twice as likely to show increasing amplitude toward lower frequencies compared to the case that no such trend is evident because the HVSRs are defined as the ratio of the two horizontal components to the vertical component.

When HVSRs exhibit increasing amplitude toward lower frequencies, it is not sufficient to simply find the frequency with the highest absolute amplitude to identify the peak associated with the shallow subsurface (red arrow in the figure). Accordingly, the following procedure was used in this study to identify the peak frequency. First, we identified all local peaks within the frequency range $[f_{ll}, f_{ul}]$. Each peak was then paired with the trough located on its high-frequency side, and a score was evaluated for each peak–trough pair using the following equation

$$SCORE_i = SRP_i/SRT_{\min} + W \cdot SRP_i/SRT_i, \quad (1)$$

where the subscript i refers to the ith local peak. SRP_i and SRT_i denote the amplitudes of the peak and the corresponding trough, respectively (Fig. 6). $SRT_{\min}$ is the minimum value among all SRT_i ($i = 1, \ldots$). W is a weighting factor applied to the peak–trough amplitude ratio SRP_i/SRT_i. This weight is a constant that does not depend on the observation point or on the peak index. A score was calculated for each local peak using this equation. The peak with the highest score was then selected as the representative peak of the spectrum, and its corresponding frequency was taken as f_p.

In bedrock or in hard ground similar to bedrock, it is expected that either no peak will occur in the HVSR or, if a peak does occur, it will occur at a high frequency. In such cases, we used the peak–trough ratio SRP_i/SRT_i as an indicator of peak prominence. When this ratio did not exceed a prescribed threshold R_{ll}, the peak was regarded as insufficiently distinct and was excluded from the score evaluation. For sites where no peak was identified using this criterion, the upper frequency limit f_{ul} was assigned as a nominal value for f_p.

When evaluating the scores, the influence of spectral trends can be reduced by assigning an appropriate value to W. Setting W to 0 means selecting the global maximum of the spectrum. Assigning a value to W that is too high may lead to the extraction of local peaks that are physically meaningless because the overall spectral shape is effectively ignored. Assigning a value to the peak-prominence threshold R_{ll} that is too large increases the number of sites classified as having "no peak," potentially causing important data to be overlooked. Conversely, if the value assigned to R_{ll} is too low, even

noise-induced fluctuations may be misidentified as local peaks, hindering the extraction of peaks associated with shallow subsurface structure.

These peak-selection parameters must be determined while keeping the above issues in mind through a process of trial and error that involves visually checking the overall spectral shape and preparing provisional peak-frequency maps (hereafter, f_p maps) as needed. In this study, W = 4.0 and R_{ll} = 4.0 were assigned as final parameter values. The rationale for these choices is described later in Section 6.5.

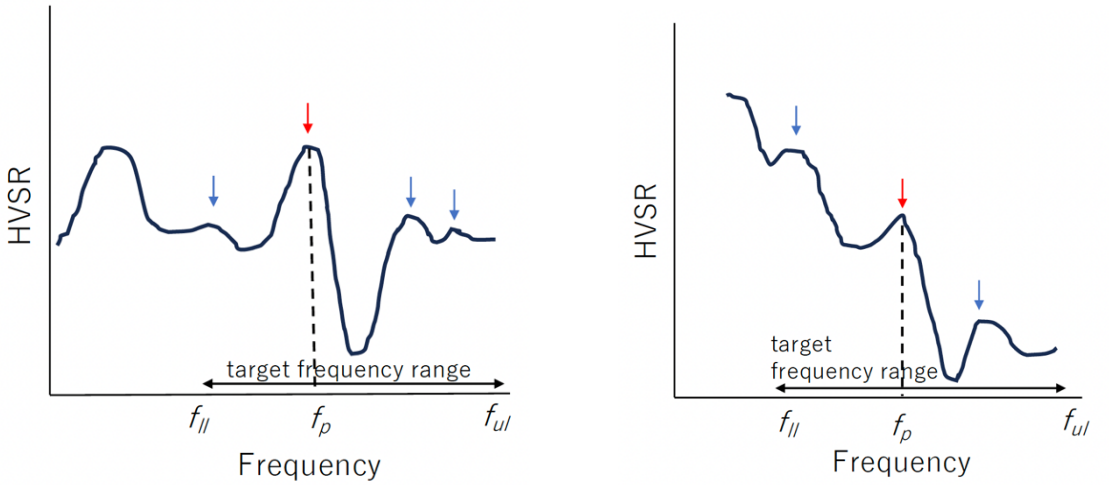

(a) Example of no frequency dependence of amplitude

(b) Example of amplitude increasing with decreasing frequency toward caused by underlying factor

Fig. 5 Factors interfering with identification of HVSR peaks. Arrows indicate local peaks. Conceptual illustration shown on log–log scale.

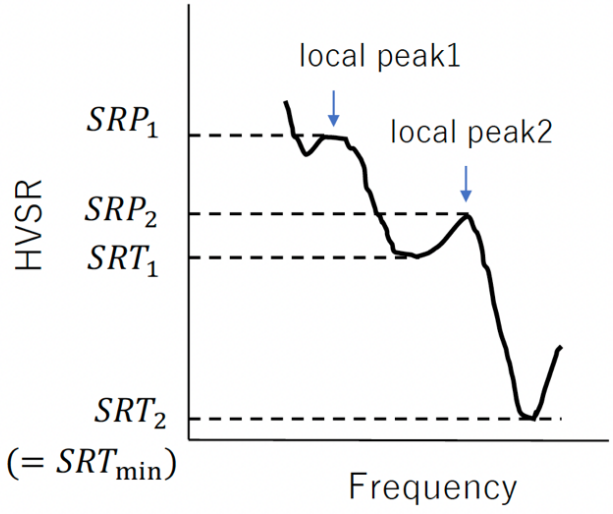

Fig. 6 Score evaluation using peak–trough amplitude data for each local peak in Eq. (1). Conceptual illustration shown on log–log scale.

6. RESULTS

6.1 Topography

HVSRs and f_p were evaluated for all microtremor measurement sites (Fig. 4) using the procedures described in the previous chapter. Figure 7 shows the average HVSRs for representative areas of (a) lowlands, (b) uplands (terraces), and (c) valley-bottom lowlands. For (a) and (b), all observation points within the selected areas were included; while for (c), sites were chosen in consideration of the local topography. From the figure, it is evident that f_p increases in order from the lowlands (0.93 Hz) to uplands (4.0 Hz) and valley-bottom lowlands (10 Hz). These differences in f_p are thought to reflect the thickness of the soft surficial layer, which decreases in the order from lowlands to uplands and valley-bottom lowlands. Even within areas classified as "lowlands," f_p can differ substantially, as seen for the soft-sediment lowlands in (a) and valley-bottom lowlands in (c), where most of the soft deposits have been removed by fluvial erosion.

Figure 8 shows the spatial distribution of f_p. From Fig. 8(a), it is apparent that the f_p patterns for the Arakawa and Nakagawa Lowlands differ from those of the Omiya Upland. The Nakagawa and Arakawa Lowlands and surrounding areas appear in red, suggesting the presence of soft ground. In contrast, the Omiya Upland is generally green with some bluish areas, indicating that the ground conditions are "good" to "intermediate." In Fig. 8(b), the distributions of low-f_p and high-f_p zones are delineated by the iso-frequency contours showing the 1.7-Hz threshold (dark red) for "soft ground" and the 5.0-Hz threshold (dark blue) for "good ground." Figure 8(c) shows only these iso-frequency contours, drawn based on the distribution. Figure 8(d) overlays the iso-frequency contours from (c) onto the topographic map from Fig. 7. The locations of rectangles a, b, and c from Fig. 7 are shown to visualize the representative HVSRs associated with each color-coded region.

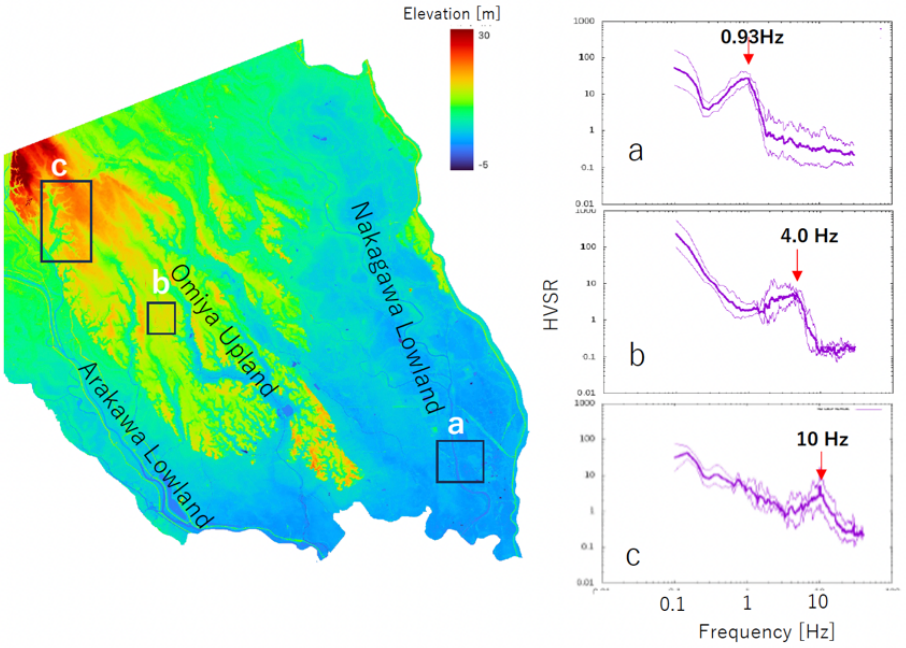

Fig. 7 Relationship between topography and HVSR. Bold lines represent the average and thin lines represent the standard deviation. Red arrows and numerical labels indicate the peak locations and corresponding f_p. The latitude, longitude, and scale are the same as those for Fig. 4.

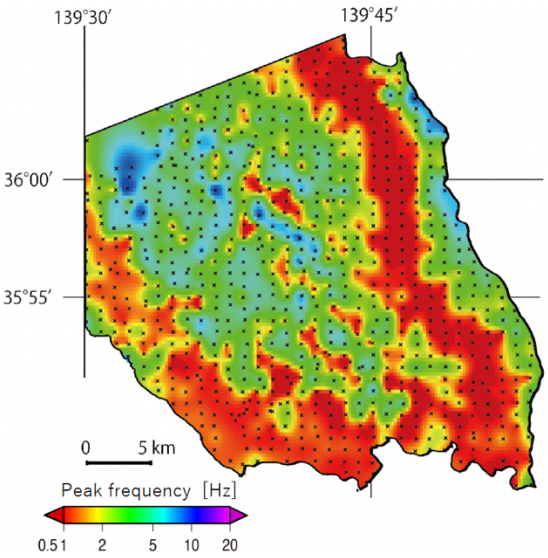

(a) Distribution of peak frequency (f_p) in model area (crosses represent microtremor measurement sites)

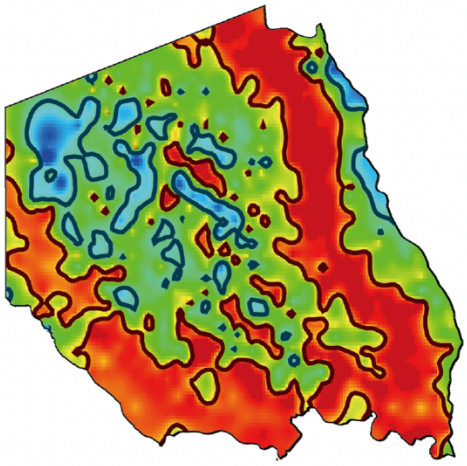

(b) Map (a) overlain with frequency contour lines (dark red line = 1.7 Hz; dark blue line = 5.0 Hz)

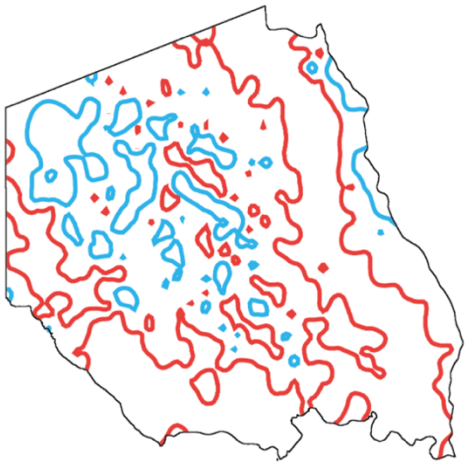

(c) Contour lines extracted from panel (b) (colors have been modified to improve readability)

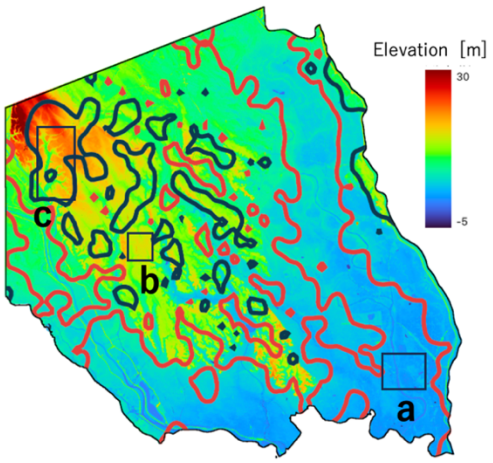

(d) Contour lines from panel (c) overlain on Fig. 7 (a, b, and c replicate the rectangular areas in Fig. 7)

Fig. 8 Spatial distribution of peak frequency (f_p) in model area

6.2 Alluvium

Figure 9 overlays the f_p distribution from Fig. 8(c) onto the spatial distribution of alluvium thickness derived from the UGmap (calculated as the difference between the ground-surface elevation and the elevation of the alluvial basal surface). The figure shows close correspondence between areas with thick alluvium in the Arakawa and Nakagawa Lowlands and the distribution of low f_p values (red contours). Across the entire region underlain by alluvium, the average f_p is 1.9 ± 1.4 Hz (range expressed as one standard deviation). If only areas with thicker alluvium (for example, where the alluvium thickness exceeds 20 m) are examined, the average f_p is 1.3 ± 0.7 Hz. At least half of these sites fall into what is commonly classified as soft ground.

For a two-layer ground model, the resonant frequency f_0 is related to the S-wave velocity V_s and thickness H of the upper layer according to the following equation, known as the 1/4-wavelength rule[25]:

$$H = V_s/(4f_0). \tag{2}$$

The above equation can be interpreted as indicating that H and f_0 are inversely related if the alluvium is a soft layer with approximately constant V_s. Accordingly, the relationship between f_p obtained from microtremor measurements at sites underlain by alluvium and its thickness H derived from the UGmap is shown in Fig. 10. The values are shown as relative frequencies to highlight overall trends. Following previous studies[26], theoretical curves were also plotted for three representative V_s values—100, 150, and 200 m/s—used in Eq. (2), corresponding to lines 1, 2, and 3, respectively. The figure shows that, for the alluvium within the model area, the relationship between the resonant frequency f_p derived from microtremor measurements and the alluvial thickness H based on the UGmap is generally consistent with Eq. (2).

The alluvial lowland (AL in Fig. 9) in the central-northern part of the model area is known to have a thinner alluvium than the axial zone of the Nakagawa Lowland located to its east. If we assume that the alluvium in this area has a V_s in the range 100–200 m/s and a thickness of 3–5 m, then Eq. (2) yields a resonant frequency of approximately 5.0–17 Hz. However, the observed f_p values in this region generally fall within the range of 1.7–5.0 Hz (i.e., between the blue and red contours). Therefore, it appears that the f_p values in this region are not primarily driven by the alluvium (see Section 6.3 for further discussion).

Alluvium is also found in the valleys incised into the Omiya Upland (i.e., valley-bottom lowlands). The geological characteristics of valley-bottom lowlands typically differ between the upper, middle, and lower reaches of a valley. While the alluvium in the upper reaches is thin or may be absent altogether, it tends to be thicker in the lower reaches, with corresponding f_p values[27]. The low-f_p zones labeled L1 in Fig. 9 (three locations corresponding, from north to south, to the Moto-Arakawa, Ayase, and Shibakawa River basins) are therefore interpreted as reflecting the increase in thickness of alluvium within valley-bottom lowlands.

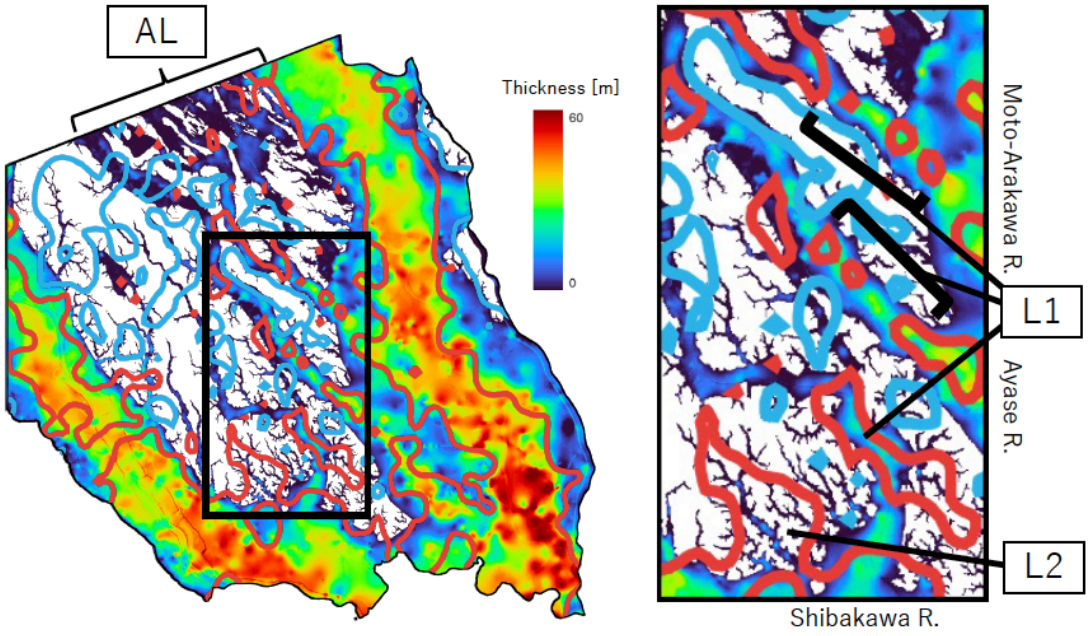

Fig. 9 Alluvium thicknesses derived from the UGmap. To facilitate comparison with the f_p distribution, the map is overlain with the iso-frequency contours from Fig. 8(c). Latitude, longitude, and scale are the same as in Fig. 4. The right panel is a close-up of the rectangular area indicated in the left panel.

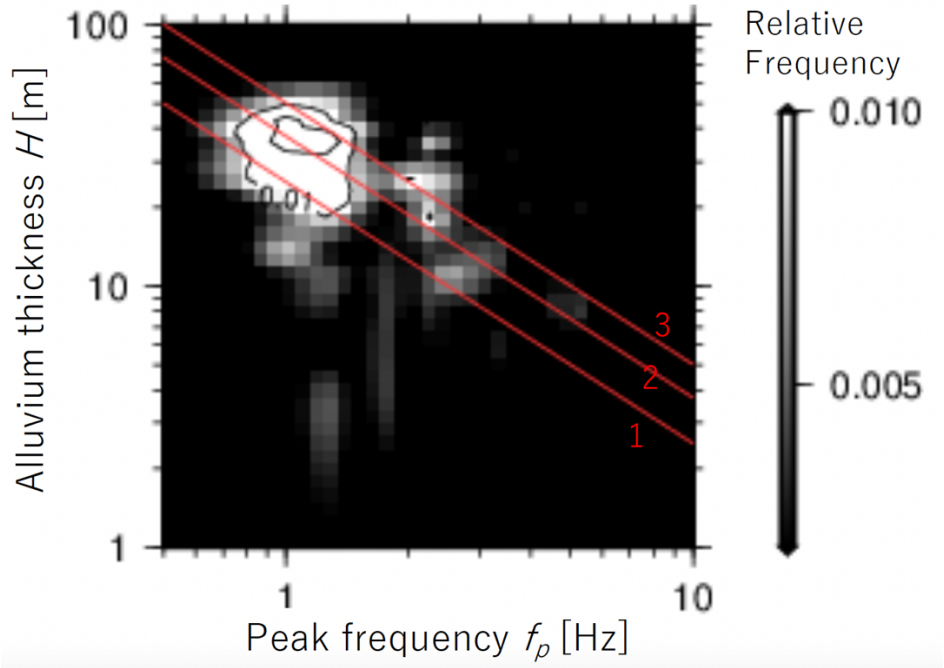

Fig. 10 Relationship between peak frequency (f_p) and alluvium thickness H derived from UGmap (Relative frequency; total number of data points = 633). Red lines 1, 2, and 3 represent the theoretical values obtained from Eq. (2) for V_s = 100, 150, and 200 m/s, respectively.)

6.3 From the ground surface to the Omiya Formation and the upper part of the Kioroshi Formation

The average f_p for areas without alluvium is 4.7 ± 2.1 Hz, which is approximately 2.5 times the average value for areas underlain by alluvium. Given the relationship expressed in Eq. (2), this result suggests that in regions without alluvium, the near-surface low-V_s layer (consisting primarily of the Kanto Loam Bed or the Omiya Formation) is either relatively thin, has a higher V_s, or both.

Figure 11 shows the distribution of the thickness of the strata from the ground surface down to the basal surface of the Omiya Formation, based on the UGmap. In areas underlain by alluvium, the values represent the combined thickness of the alluvium and the Omiya Formation; in the uplands, they represent the combined thickness of the Kanto Loam Bed and the Omiya Formation. This composite layer is relatively thick (> 15 m) (Fig. 11) and overlies a thick section of the upper part of the Kioroshi Formation (Fig. 12). These relatively softer portions within the stratigraphic sequence are thought to act collectively as the upper layer of a "two-layer ground model," controlling the local ground response characteristics of this region. Both Figs. 11 and 12 are overlain by the f_p distribution from Fig. 8(c) and show that f_p generally falls within the range 1.7–5.0 Hz, with some areas exceeding 5.0 Hz. For example, f_p exceeds 5.0 Hz on the northern terrace surface between the Moto-Arakawa and Ayase Rivers (the Iwatsuki Terrace; Fig. 1), suggesting relatively "good" ground conditions (H1 in Fig. 11).

In the upper reaches of the valleys, there are areas where the alluvium has been eroded and the Omiya formation has also become thin. Because such zones tend to be limited in extent, they are difficult to detect as distinct areas given the grid spacing of our microtremor measurement (1-km mesh). However, while these zones are concentrated to some degree, their presence is nonetheless suggested by the f_p map (e.g., H2 in Fig. 11).

6.4 Lower part of the Kioroshi Formation

In L2 of Fig. 9, the f_p values are low even though very little soft alluvium is present. One possible reason for this is that the lower part of the Kioroshi Formation is thickly developed in this area (Kil1 in Fig. 13). Because the lower part of the Kioroshi Formation consists of soft mud layers with low V_s, it can yield low f_p values even though alluvium is not present. In fact, in areas where the lower part of the Kioroshi Formation is thick, HVSRs tend to exhibit a peak at around 1 Hz.

In contrast, the overlying units (the upper part of the Kioroshi Formation, the Omiya Formation, and the Kanto Loam Bed) tend to produce a characteristic peak for this upland in the 4–5 Hz range or higher frequencies—regardless of the presence of the lower part of the Kioroshi Formation (Figs. 7 and 8). As a result, in areas where the lower part of the Kioroshi Formation is present, two peaks generated by the shallow subsurface occur together (Kil1 and Kil2 in Fig. 13). Because the peak amplitudes vary depending on the combination of layer thicknesses and their average V_s values, it is not consistent which of the two peaks has the higher amplitude. For example, in the area surrounding Kil1 in Fig. 13, the lower-frequency peak is selected as the representative peak, resulting in classification as a low-f_p zone (highlighted by the red frame). In contrast, in the area around Kil2—which is proximal to Kil1—the higher-frequency peak is selected, and accordingly, the area is not classified as a low-f_p zone.

As noted above, according to the peak-selection procedure described in Section 5.2, when multiple peaks exhibit comparable prominence, all but one are disregarded. This is an inherent limitation of the mapping-based approach, which is designed to allow the spatial distribution of f_p to be visualized at a glance.

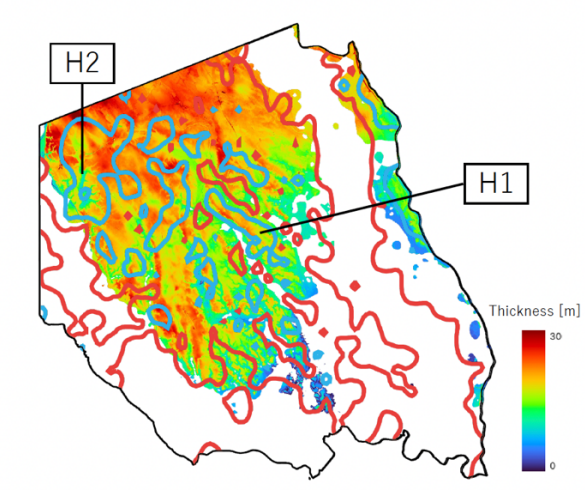

Fig. 11 Thickness of stratigraphic sequence from ground surface to the base of the Omiya Formation, based on UGmap. The map is overlain with the iso-frequency contours from Fig. 8(c) to enable comparison with the f_p distribution. Latitude, longitude, and scale are the same as in Fig. 4.

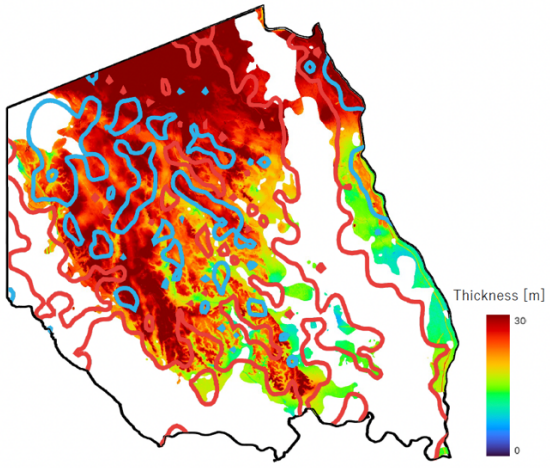

Fig. 12 Thickness of stratigraphic sequence from ground surface to base of the upper part of the Kioroshi Formation, based on UGmap. The map is overlain with the iso-frequency contours from Fig. 8(c) to enable comparison with the f_p distribution. Latitude, longitude, and scale are the same as in Fig. 4.

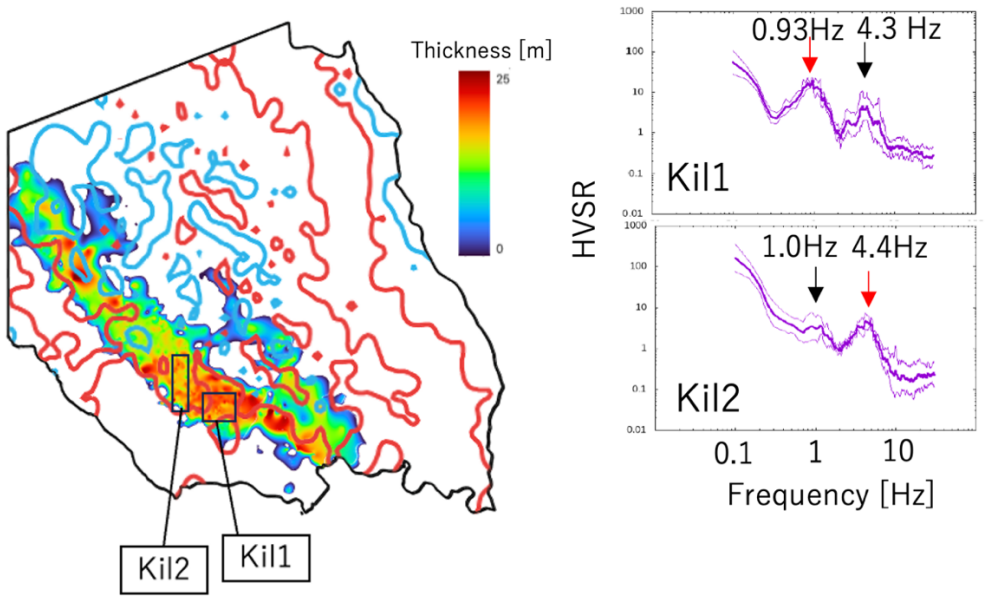

Fig. 13 Thickness and HVSRs for the lower part of the Kioroshi Formation. To facilitate comparison of the f_p distribution, the map is overlain with the iso-frequency contours from Fig. 8(c). The latitude, longitude, and scale are the same as in Fig. 4.

6.5 Rationale for parameter values adopted for peak selection

In the above sections (Sections 6.1 to 6.4), we examined the relationship between geology and f_p values based on the f_p map generated with W = 4.0 and R_{ll} = 4.0 (Section 5.2) as set values for the peak selection parameters. In this section, we explain the rationale behind these parameter values.

We first consider how the peak-selection parameters influence the overall appearance of the f_p map. Figures 14 and 15 show f_p maps generated by varying both W and R_{ll} using the values 0.0, 2.0, 4.0, 6.0, 8.0, and 10.0. Setting W = 0 and R_{ll} = 0 (panels framed in blue) is equivalent to not using these parameters—that is, simply treating the maximum spectral amplitude as the spectral peak. The panels framed in red indicate the parameters adopted in this study (W = 4.0 and R_{ll} = 4.0). As can be seen, varying these parameters does not dramatically change the overall appearance of the f_p map. In principle, when the HVSRs do not contain multiple local peaks (i.e., there is a single dominant peak), the f_p map is unaffected by peak-selection parameters. The strongly reddish zones along the buried-valley axes of the Arakawa and Nakagawa Lowlands are examples of this case. In contrast, as the HVSRs for the Omiya Upland and surrounding areas tend to exhibit multiple local peaks, the choice of parameters affects which peak is selected. Specifically, assigning smaller values to both W and R_{ll} tends to result in selection of the lower-frequency peak. This tendency is particularly pronounced when both W and R_{ll} are set to 0, resulting in the f_p map being generally biased toward lower frequency (i.e., appearing more reddish overall). The reddish color diminishes somewhat when either W or R_{ll} is set to 2.0. Note, W appears to have a stronger effect on the f_p map than R_{ll}. When W and R_{ll} reach values of 4.0 or higher, further increases in parameter values result in only minor changes to the overall appearance of the map.

Next, let us examine how the peak-selection parameters affect individual HVSRs. Figure 16 shows examples of HVSRs obtained for the Iwatsuki Terrace (location shown in Fig. 1; the area also closely matches zone H1 in Fig. 11). In all four examples in the figure, the spectra exhibit increasing amplitude with decreasing frequency (Section 5.2). In all cases, local peaks appear to be superimposed on this trend at around 0.1–0.5 Hz or 1 Hz and above 6 Hz. The 7.9-Hz peak observed for SITM01045 is clearly dominant and results in the simple selection of the maximum spectral amplitude as the representative frequency in the 0.5–20 Hz target band. Given the continuity of the surrounding geology, it would be reasonable to assume that the local peaks between 6 and 10 Hz at the other three sites are generated by the same subsurface conditions as the 7.9-Hz peak at SITM01045. These peaks can thus be interpreted as reflecting the relative “good ground” conditions of the shallow subsurface of the Iwatsuki Terrace. Accordingly, we would like to select these peaks as those associated with the shallow layers down to several tens of meters. However, in the case of SITM00967, simply taking the maximum amplitude (i.e., W = 0, R_{ll} = 0) results in the low-frequency peak at 1.3 Hz being selected due to the aforementioned tendency toward higher amplitudes at lower frequencies. Therefore, it is necessary to assign appropriate values to W and R_{ll}. In this case, setting W and R_{ll} to $\geq$ 2.0 resulted in selection of the higher-frequency peak at 6.2 Hz. In the figure, the numbers shown in parentheses next to each local peak indicate the parameter combinations (W, R_{ll}) resulting in selection of this peak. For simplicity, W and R_{ll} were varied at the same increment of 2.0 (values of 0.0, 2.0, 4.0,…).

Figure 17 presents examples of HVSRs obtained for the Katayanagi Terrace (Fig. 1). As in the case of Fig. 16, all four examples exhibit increasing amplitude with decreasing frequency, with local peaks superimposed on this trend near 0.5 Hz or 1 Hz and around 4–6 Hz. In all four examples, setting W and R_{ll} to 0.0 resulted in selection of the peak near 1 Hz. However, as with SITM00967 in Fig. 16, assigning values of 2.0 or greater—or 4.0 or greater—to W and R_{ll} resulted in the selection of peaks in the 4–6 Hz range.

A standard borehole, GS2012-OMY (Fig. 1), is located within 2 km of the microtremor measurement sites shown in Fig. 17. The validity of the above-described peak selection procedure is supported by an interpretation that combines information on the geological structure derived from the standard borehole

data[16] and velocity logging data for the same location obtained from an independent source[28]. First, the stratigraphic information describes the Omiya Formation as appearing below the Kanto Loam Bed at a depth of 5.2 m, followed by the upper part of the Kioroshi Formation at a depth of 20.0 m (Fig. 18a). Corresponding V_s values and depth ranges based on the suspension velocity logging data show (i) a low-velocity range of 80–170 m/s extending from the Kanto Loam Bed down into the mud layer of the upper Omiya Formation (shallower than 6 m), (ii) discontinuous increases to 205 m/s and 240 m/s at 6 m and 8 m depth, respectively, corresponding to the upper boundary of the sandy layer within the Omiya Formation, and (iii) gradual increases in V_s values from 11 m to 15 m depth, followed by values that, despite some disturbance, remain approximately constant at around 350 m/s down to 100 m depth.

Based on the above data, inputting average V_s values from the ground surface down to depths of 6 m and 8 m into Eq. (2) yields resonant frequencies of 5.7 Hz and 4.7 Hz, respectively. In fact, the HVSR recorded at a site located approximately 10 m from the borehole site shows a distinct peak at 5.2 Hz (Fig. 18(b)). This result suggests that these velocity discontinuities contribute to the formation of this peak. It should be noted that, although the HVSR for this site did not show a trend of increasing amplitude with decreasing frequency as seen in Figs. 16 and 17, a local peak exists near 1 Hz. If this spectrum exhibited a trend similar to those seen in Figs. 16 and 17, it is possible that the local peak around 1 Hz would instead be selected.

Considering the continuity of the geological structure (Fig. 18(c)), the 4–6 Hz peak observed at the microtremor measurement sites in Fig. 17 can be interpreted as reflecting a subsurface structure of roughly the same scale as this location—namely, the depth range extending from the Kanto Loam Bed through the Omiya Formation. Meanwhile, based on the resonant-frequency estimates derived from Eq. (2), it is likely that the weak peaks near 1 Hz observed in the HVSRs in Figs. 18(b) and 17 reflect subsurface structures at a depth of 100 m or greater. The peak near 1 Hz in Fig. 16 is probably attributable to the same source.

As discussed above, when W and R_{ll} are assigned values of 4.0 or greater, the overall appearance of the f_p map remains largely unchanged, indicating that the results are strongly influenced by the shallow subsurface structure down to several tens of meters. The inherent arbitrariness of the procedure suggests that, whenever possible, smaller values should be used for peak-selection parameters. Taking these considerations into account, in this study, we assigned $W = 4.0$ and $R_{ll} = 4.0$ as parameter values. Note that the detailed features of the resulting map are sensitive to the arbitrary parameter settings, particularly in upland/terrace areas.

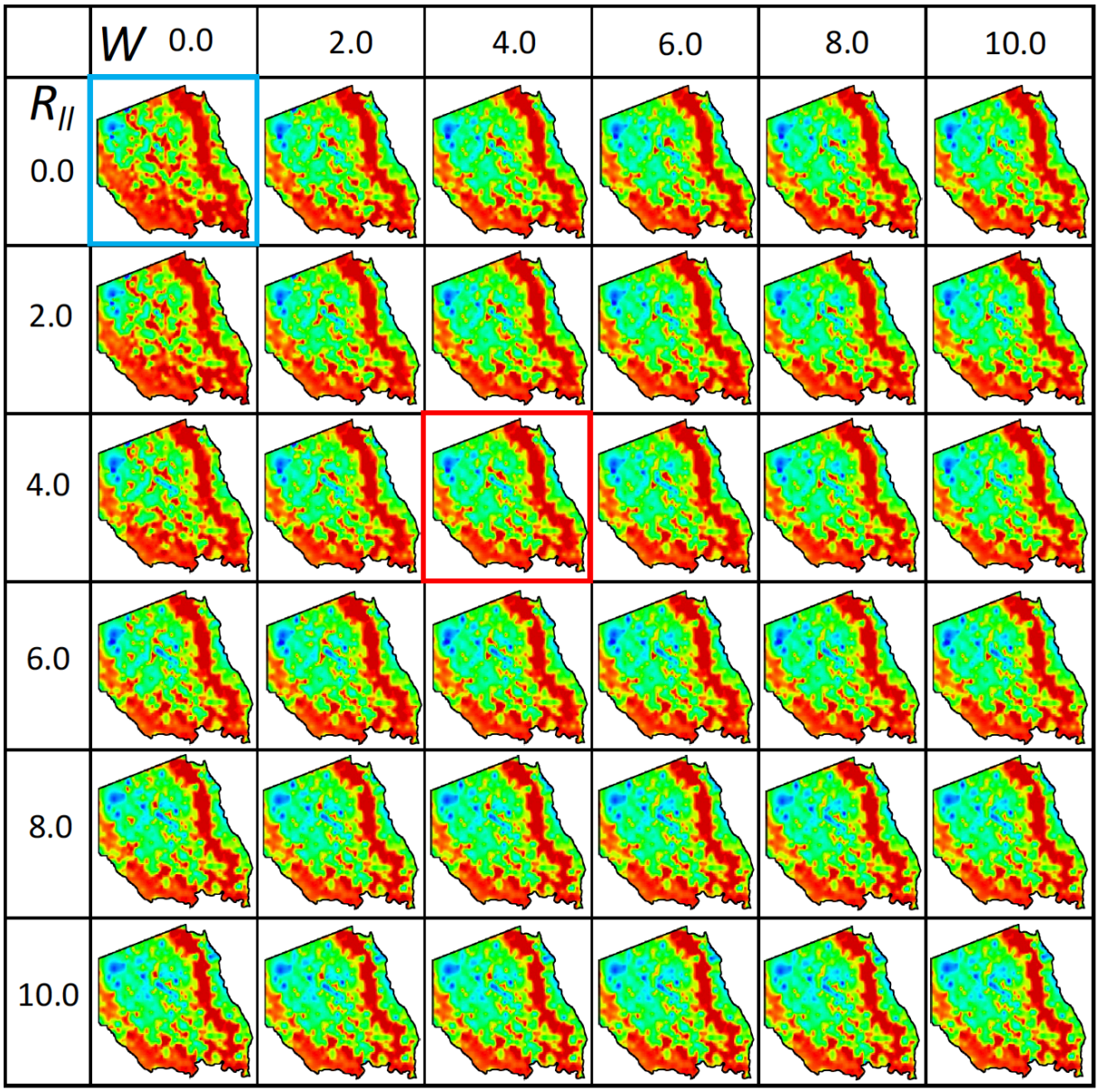

Fig. 14 Peak frequency maps for different values of peak-selection parameters W and R_{II} (color-coded maps: the legend is the same as in Fig. 8)

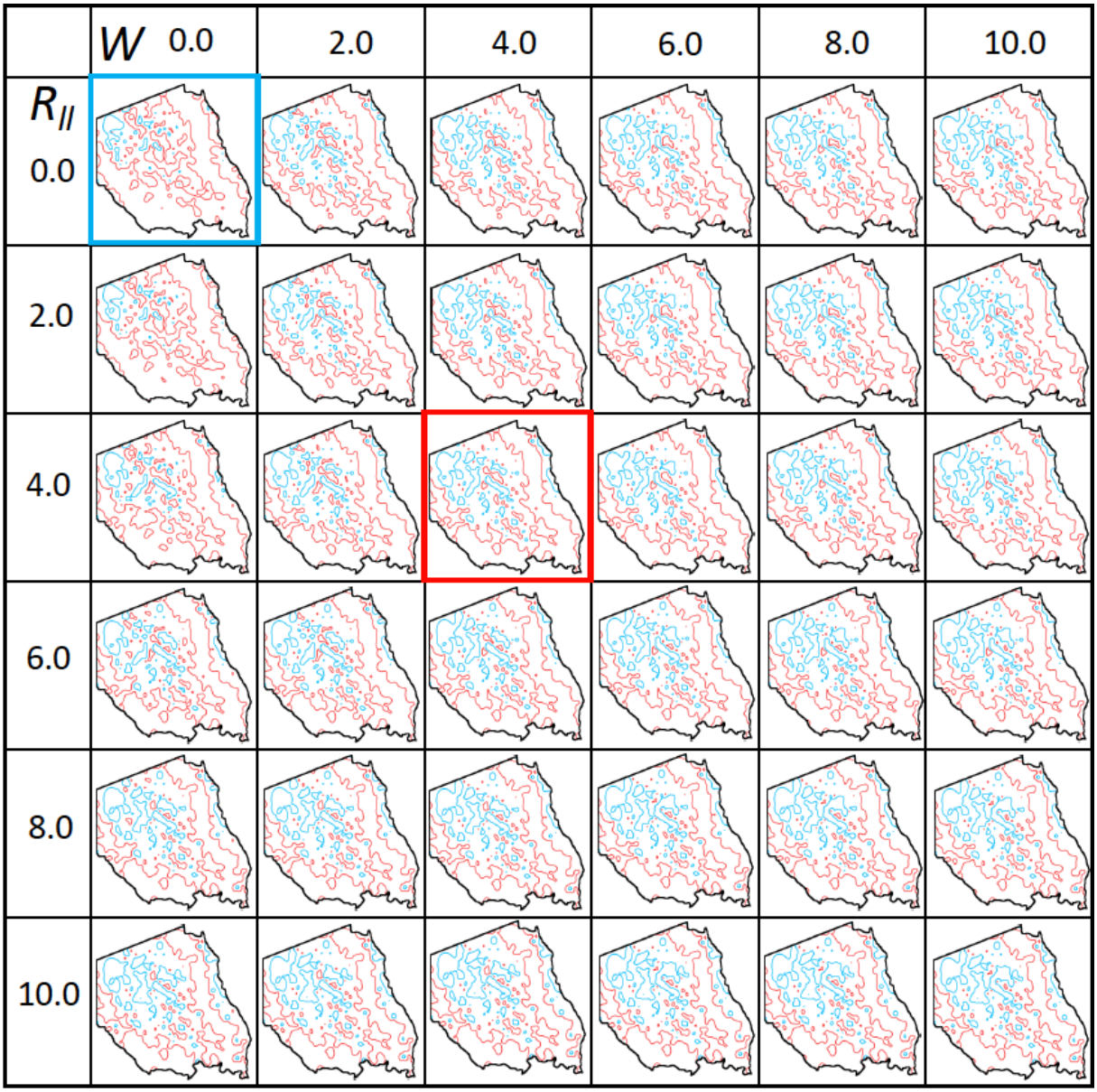

Fig. 15 Peak frequency maps for different values of peak-selection parameters W and $R_{//}$ (iso-frequency contour maps: red lines = 1.7 Hz, blue lines = 5.0 Hz)

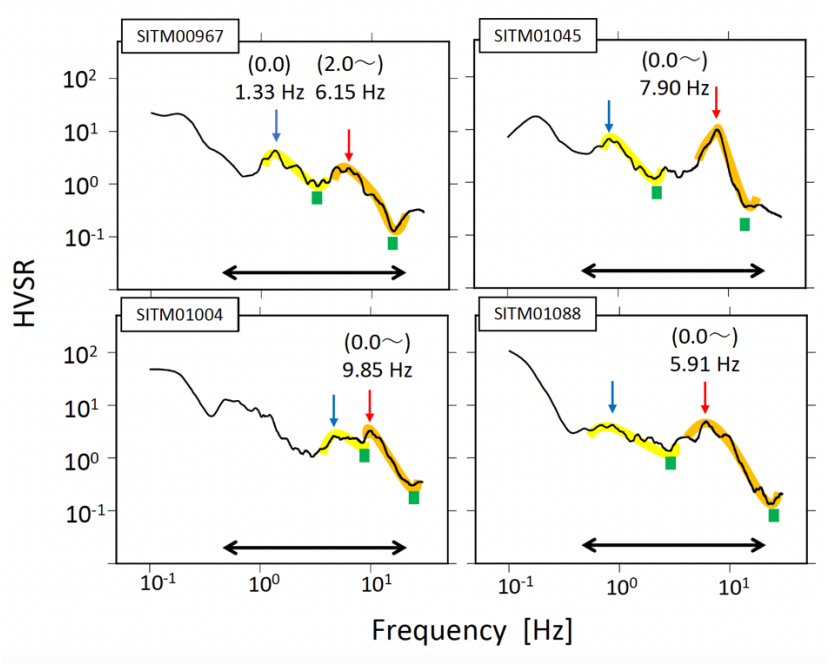

Fig. 16 HVSRs for Iwatsuki Terrace. Vertical arrows indicate local peaks, with the peaks selected in this study indicated by red arrows. Squares mark the positions of the troughs; in this study, scores were evaluated for one-to-one corresponding peak–trough pairs. Numbers above vertical arrows represent the peak frequencies f_p. Numbers in parentheses are the values of the peak-selection parameters W and R_{ll} resulting in selection of that local peak. Horizontal arrows indicate the analyzed frequency range of 0.5–20 Hz. The thick colored lines tracing segments of the spectra indicate the authors' interpretations of peaks and troughs; the colors themselves carry no meaning.

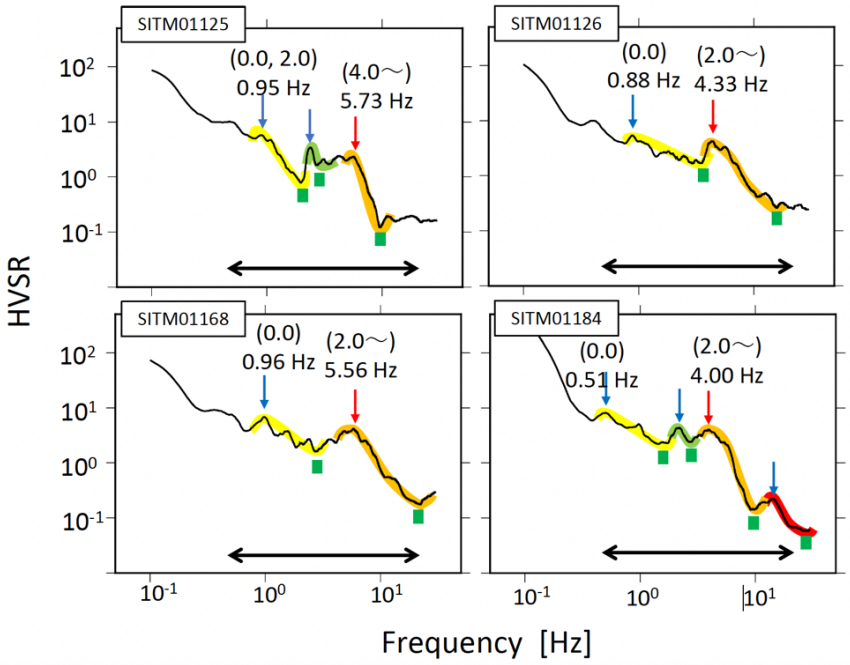

Fig. 17 HVSRs for Katayanagi Terrace (the legends are the same as in Fig. 16)

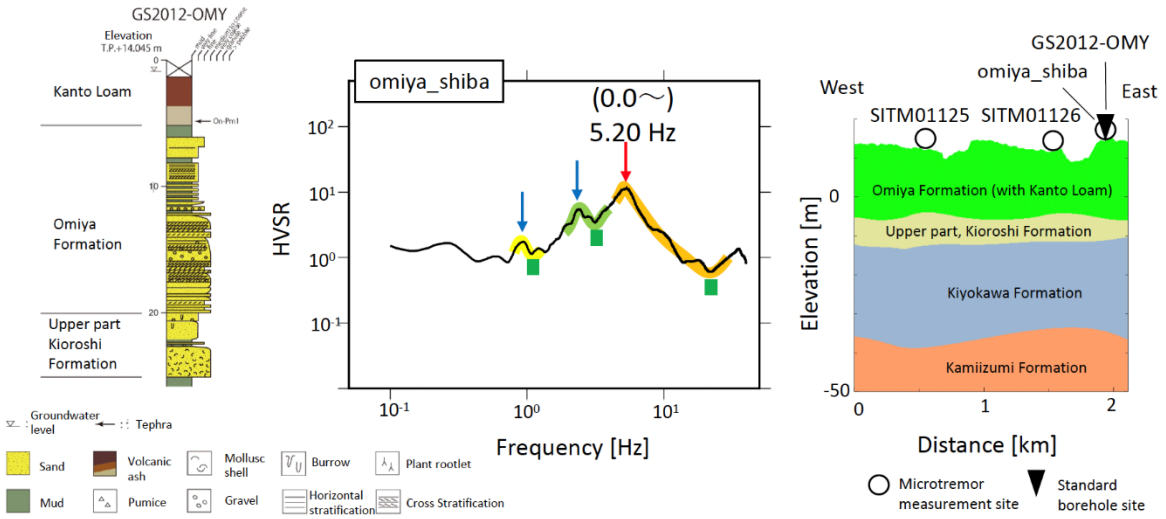

(a) Geological column (partial reproduction of online UGmap[16])

(b) HVSR (the legend is the same as in Fig. 16)

(c) Geological cross-section modified from online UGmap[16]. The triangle indicates a standard borehole site, while the circles indicate microtremor measurement sites.

Fig. 18 Geological column, HVSR, and geological cross-section (east to west) for standard borehole GS2012-OMY

7. DISCUSSION AND CONCLUSIONS

During the Great Kanto earthquake of 1923, dramatic differences in damage were observed between uplands and lowlands[29], which drew attention to the alluvium of the Tokyo Lowland as a typical example of soft ground[30]. Even today, evaluations based on surface terrains are still generally considered to provide a reasonable first-order approximation of seismic hazards, as evidenced by the use of engineering geomorphologic classification as a basis for seismic hazard assessments[19]. However, there are cases where alluvial lowlands exhibit better ground characteristics than the surrounding uplands—for example, in valley-bottom lowlands[27]. Similarly, even upland areas may experience amplification of around 1-Hz ground motions (Section 3), resulting in greater risk of seismic damage, if the loam layer is thick[31), 32] or when subsurface-buried valleys influence the local structure[33]. Understanding the nature of such situations requires information about the subsurface structure. Three-dimensional subsurface structures are valuable as they can provide supplemental information that cannot be inferred from topography alone, enabling more advanced evaluations of site conditions and seismic hazards.

The peak frequencies of HVSRs can be considered quantitative indicators of the validity of qualitative speculations about ground conditions and seismic hazards inferred from topography and 3D geological/soil structure. For example, in terms of the engineering geomorphologic classification[34], the central parts of the Arakawa and Nakagawa Lowlands represent back-marshes where soft ground conditions are anticipated. Consistent with this expectation, areas where alluvium thickness exceeds 20 m in thickness exhibit an average peak frequency of approximately 1.3 Hz (corresponding to Type III ground in seismic design classifications). In contrast, although the northwestern portion of the

Nakagawa Lowland near the Omiya Upland (area AL in Fig. 9) is also mapped as back-marsh in terms of the engineering geomorphologic classification, the UGmap indicates that the alluvium in this area is substantially thinner than in the central axis of the Nakagawa Lowland, suggesting better ground conditions. Indeed, the peak frequencies observed in this region range from 1.7 to 5.0 Hz (Type II ground). The Omiya Upland exhibits better ground conditions than the Arakawa and Nakagawa Lowlands, while the ground quality of valley-bottom lowlands is expected to vary depending on catchment position. In fact, the peak frequencies for the Omiya Uplands were observed to range from 1.7–5.0 Hz (Type II ground), with peak frequencies exceeding 5.0 Hz (Type I ground) in some localized areas. In valley-bottom lowlands, peak frequencies varied in a similar fashion among drainage basins, reflecting differences in the thickness of soft layers.

As illustrated above, topography, 3D subsurface structure, and HVSRs can be regarded as fundamental datasets that complement each other and collectively inform assessments of ground conditions and seismic hazard.

When interpreting peak-frequency maps created based on HVSRs, it is important to recognize that extracting a single parameter, the peak frequency, from the spectra may fail to capture the complexity of the subsurface structure (Sections 6.4 and 6.5). It should also be noted that, in this study, the frequency band from which HVSR peak frequencies were extracted was restricted to a range that is not influenced by the deep subsurface structure (Section 5.2). This restriction is generally acceptable for the purpose of classifying ground types, since ground-type classifications are, by their nature, concerned with the shallow subsurface. However, the peak frequency maps derived from HVSRs used in this study are inadequate in situations where the influence of the deep subsurface structure needs to be taken into account, for example, when evaluating ground motions below 0.5 Hz. Low-frequency shaking by an earthquake (i.e., long-period ground motions[35]) has recently received attention due to its relevance to high-rise buildings and large-scale structures.

Based on the above considerations, this study focused on evaluating HVSR peak frequencies in southeastern area of Saitama Prefecture, for which geological ground maps have recently been released[16]. The resulting peak-frequency map will be made available on the Urban Geological Map website, enabling users to zoom in and out and to conduct detailed comparisons with geological units. We plan to generate and publish similar peak-frequency maps for other regions in the future.

ACKNOWLEDGMENT

This manuscript was greatly improved by the comments provided by three anonymous reviewers. In particular, the latter part of Section 2, Section 6.5, and the related figures were newly incorporated in response to their suggestions. The authors express our sincere gratitude for their valuable contributions.

REFERENCES

1) Okada, H.: *The Microtremor Survey Method, Geophysical Monograph Series (Vol. 12)*, Society of Exploration Geophysicists, 135 pp., Tulsa, OK, 2003.
2) Society of Exploration Geophysicists of Japan (SEGJ), *Handbook of Geophysical Survey Methods* (Enlarged and Revised Edition), SEGJ, pp. 229–248, 2016 (in Japanese, title translated by the authors).
3) Nogoshi, M. and Igarashi, T.: On the Amplitude Characteristics of Microtremor (Part 2), *Zisin 2*, Vol. 24, pp. 26–40, 1971 (in Japanese).
4) Japan Road Association, ed.: *Specifications for Highway Bridges, Part V Seismic Design*, Maruzen

Shoten, 302 pp., 2017 (in Japanese, title translated by the authors).
5) Ohmachi, T., Konno, K., Endoh, T. and Toshinawa, T.: Refinement and Application of an Estimation Procedure for Site Natural Periods Using Microtremor, *Japanese Journal of Japan Society of Civil Engineering*, No. 489/I-27, pp. 251–260, 1994 (in Japanese).
6) Konno, K. and Ohmachi, T.: Ground-Motion Characteristics Estimated from Spectral Ratio between Horizontal and Vertical Components of Microtremor, *Bulletin of the Seismological Society of America*, Vol. 88, pp. 228–241, 1998.
7) Architectural Institute of Japan, ed.: *Earthquake Ground Motion–Phenomena and theory–*. Architectural Institute of Japan, pp. 283–295, 2005 (in Japanese, title translated by the authors).
8) Senna, S., Midorikawa, S. and Wakamatsu, K.: Estimation of Spectral Amplification of Ground Using H/V Spectral Ratio of Microtremors and Geomorphological Land Classification, *Journal of Japan Association for Earthquake Engineering*, Vol. 8, pp. 1–15, 2008 (in Japanese).
9) Arai, H. and Tokimatsu, K.: S-Wave Velocity Profiling by Inversion of Microtremor H/V Spectrum, *Bulletin of the Seismological Society of America,* Vol. 94, No. 1, pp. 53–63, 2004.
10) Arai, H. and Tokimatsu, K.: S-Wave Velocity Profiling by Joint Inversion of Microtremor Dispersion Curve and Horizontal-to-Vertical (H/V) Spectrum, *Bulletin of the Seismological Society of America*, Vol. 95, pp. 1766–1778, 2005.
11) Senna, S., Fujiwara, H., Maeda, T., Morikawa, N., Iwaki, A., Kawai, S., Yatagai., A., Sato., T., Suzuki, H., Inagaki, Y. and Matsuyama, H.: Modeling of the Subsurface Structure from the Seismic Bedrock to the Ground Surface for a Strong Motion Evaluation, *Technical Note of the National Research Institute for Earth Science and Disaster Resilience*, No. 498, 259 pp., 2023 (in Japanese).
12) Nakazawa, T., Nonogaki, S. and Miyachi Y.: Three-Dimensional Urban Geological Map—New Style of Geoinformation in an Urban Area, *Synthesiology* (English Edition), Vol. 9, No. 2, pp. 74–86, 2016.
13) Nonogaki, S. and Nakazawa, T.: Development of Three-Dimensional Geological Maps in Urban Plane area and Its Utilization, *Journal of the Japan Society of Engineering Geology*, Vol. 65, No. 6, pp. 259–266, 2025 (in Japanese).
14) Naya, T., Nonogaki, S., Komatsubara, J., Miyachi, Y., Nakazawa, T., Kazaoka, O., Shiozaki, S., Kagawa, J.,Yoshida, T., Kato, A., Yabusaki, H., Ogitsu, T. and Nakazato, H.: *Explanatory Text of the Urban Geological Map of the Northern Area of Chiba Prefecture*, Geological Survey of Japan, AIST, 55 pp., 2018 (in Japanese).
15) Naya, T., Komatsubara, J., Nonogaki, S., Ozaki, M., Miyachi, Y., Nakazawa, T., Nakazato, H., Suzuki, T. and Nakayama, T.: *Explanatory Text of the Urban Geological Map of Central Tokyo (Special Wards Area)*, Geological Survey of Japan, AIST, 82 pp., 2021 (in Japanese).
16) Yoneoka, K., Nonogaki, S., Komatsubara, J., Ozaki, M., Nakazato, H., Nakazawa, T. and Hachinohe, S.: *Explanatory Text of the Urban Geological Map of the Southeastern Area of Saitama Prefecture*, Geological Survey of Japan, AIST, 74 pp., 2025 (in Japanese).
17) Editorial Committee of Earthquake Ground Motion, ed.: *Earthquake Ground Motion*, Geotech Note 9, Japanese Geotechnical Society, 116 pp., 1999. (in Japanese, title translated by the authors)
18) Bonnefoy-Claudet, S., Köhler, A., Cornou, C., Wathelet, M. and Bard, P. -Y.: Effects of Love Waves on Microtremor H/V Ratio, *Bulletin of the Seismological Society of America*, Vol. 98, pp. 288–300, 2008.
19) Earthquake Research Committee, the Headquarters for Earthquake Research Promotion: *Procedures to Build a Subsurface Velocity Structure Model*, 19 pp., 2017 (Translated in 2022). https://www.jishin.go.jp/main/chousa/17apr_chikakozo/model_concept-e.pdf (last accessed on December 23, 2025)
20) Sakai, Y.: Relationship between the Characteristics of Seismic Motions and Building Damage, *Journal of Japan Association for Earthquake Engineering*, Vol. 9, pp. 12–19, 2009 (in Japanese, title translated by the authors).
21) Bendat, J. S. and Piersol, A. G.: *Random Data: Analysis and Measurement Procedures* (4th ed.), Wiley, 604 pp., 2010.
22) Cho, I., Tsurugi, M., Kagawa, T. and Iwata, T.: Modeling Deep Sedimentary Velocity Structures for Evaluation of Broadband Strong Ground Motions: Site-Amplification Spectra in Osaka

Sedimentary Basin, *Journal of Japan Association for Earthquake Engineering*, Vol. 6, pp. 113–132, 2006 (in Japanese).
23) M. Stoyanov, M., Gunzburger, M. and Burkardt, J.: Pink Noise, $1/f^{\alpha}$ Noise, and Their Effects on Solutions of Differential Equations, *International Journal for Uncertainty Quantification*, Vol. 1, pp. 257–278, 2011.
24) Kobayashi, T.: Mechanism of the 1/f Noise Production, *Bulletin of Shiga University of Medical Science, General Education*, Vol. 1, pp. 1–11, 1990. (in Japanese)
25) Society of Exploration Geophysicists of Japan (SEGJ) , *Guide to the Application of Geophysical Surveys: Civil Engineering Geophysical Survey Manual 2008* (New Edition), SEGJ, 540 pp., 2008 (in Japanese, title translated by the authors).
26) Komatsubara, J., Cho, I., Sakata, K. and Nakazawa, T.: Ground Motion Characteristics and the Depth of the S-Wave Velocity Discontinuity in the Post-LGM Incised-Valley Fills beneath the Tokyo Bay Area, Central Japan, Based on Microtremor Surveys, *Journal of the Geological Society of Japan*, Vol. 128, pp. 29–42, 2022 (in Japanese).
27) Nakazawa, T., Cho, I., Komatsubara, J. and Sakata, K.: S-Wave Velocity Structures and Ground Motion Characteristics beneath Valley Bottom Lowlands: A Case Study from the Lowlands Along the Kanda and Furukawa Rivers Incising the Musashino Upland, Tokyo, Central Japan, *Journal of the Geological Society of Japan*, Vol. 130, pp. 17–33, 2024 (in Japanese).
28) Yoshimi, M., Saomoto, H., Mizuno, K. and Hosoya, T.: All-Core Drilling and Logging Survey in the Kanto Plane and Soil Test of the Pleistocene Sediments, *Geological Survey of Japan interim report*, No. 66, 185–205, 2014 (in Japanese).
29) Moroi, T. and Takemura, M.: Re-Evaluation on the Damage Statistics of Wooden Houses for the 1923 Kanto Earthquake and Its Seismic Intensity Distribution in and around Southern Kanto District, *Journal of Japan Association for Earthquake Engineering*, Vol. 16, No. 3, pp. 35–71, 2002 (in Japanese).
30) Editorial Committee of Ground of Tokyo, ed.: *Ground of Tokyo*, Geotech Note 7. Japanese Geotechnical Society, 128 pp., 1998. (in Japanese, title translated by the authors)
31) Toshinawa, T. and Yamazaki, H.: Comparison between Ground-Motion Characteristics on Plateau and Lowland Sites Based on Strong-Motion and Microtremor Observations, *Journal of the Japan Society of Civil Engineers*, No. 612/I-46, pp. 265–274, 1999 (in Japanese).
32) Nakazawa, T., Cho, I., and Sakata, K.: S-Wave Velocity Structures and Ground Motion Characteristics of Loam Terraces: The case of the Utsunomiya area, Tochigi Prefecture, Central Japan, *Journal of the Geological Society of Japan*, Vol. 126, pp. 311–326, 2020 (in Japanese).
33) Nakazawa, T., Cho, I., Sakata, K., Nakazato, H., Hongo M., Naya T., Nonogaki, S. and Nakayama, T.: Stratigraphy, Distribution Patterns, and Ground motion Characteristics of the Pleistocene Setagaya and Tokyo Formations beneath the Musashino Upland, Setagaya, Tokyo, Central Japan, *Journal of the Geological Society of Japan*, Vol. 125, pp. 367–385, 2019. (in Japanese)
34) Wakamatsu, K. and Matsuoka, M.: Update of the 250-m Mesh Landform and Geology Classification Map, *Journal of Japan Association for Earthquake Engineering*, No. 40, pp. 24–27, 2020 (in Japanese, title translated by the authors).
35) Japan Meteorological Agency: On Long-Period Ground Motion, 2025 (in Japanese, title translated by the authors). https://www.jma.go.jp/jma/kishou/know/jishin/choshuki/ (last accessed on December 24, 2025)

(Original Japanese Paper Published: November, 2025)
(English Version Submitted: January 19, 2026)
(English Version Accepted: March 24, 2026)